Journal of Hazardous Materials 217–218 (2012) 107–115

Contents lists available at SciVerse ScienceDirect

Journal of Hazardous Materials

journal homepage: www.elsevier.com/locate/jhazmat

Visible light photocatalytic activity enhancement and mechanism of $AgBr/Ag_3PO_4$ hybrids for degradation of methyl orange

Jing Cao*, Bangde Luo, Haili Lin, Benyan Xu, Shifu Chen

College of Chemistry and Materials Science, Huaibei Normal University, 100 Dongshan Road, Anhui, Huaibei 235000, China

ARTICLE INFO

Article history:
Received 29 September 2011
Received in revised form 28 February 2012
Accepted 1 March 2012
Available online 7 March 2012

Keywords:
$AgBr/Ag_3PO_4$
Anion-exchange method
Ag nanoparticles
Reaction mechanism

ABSTRACT

Novel $AgBr/Ag_3PO_4$ hybrids were synthesized via an *in situ* anion-exchange method and characterized by X-ray diffraction (XRD), field emission scanning electron microscopy (FE-SEM), energy-dispersive spectroscopy (EDS) and UV–vis diffuse reflectance spectroscopy (DRS). Under visible light ($\lambda > 420$ nm), $AgBr/Ag_3PO_4$ degraded methyl orange (MO) efficiently and displayed much higher photocatalytic activity than that of pure AgBr or Ag_3PO_4. X-ray photoelectron spectroscopy (XPS) suggests that $AgBr/Ag_3PO_4$ transformed to be $Ag@AgBr/Ag_3PO_4@Ag$ system while remained good photocatalytic activity after 5 times of cycle experiments. In addition, the quenching effects of different scavengers proved that reactive $^{\bullet}OH$ and h^+ played the major role for the MO degradation. The photocatalytic activity enhancement of $AgBr/Ag_3PO_4$ is closely related to the efficient separation of electron–hole pairs derived from the matching band potentials between AgBr and Ag_3PO_4, as well as the good electron trapping role of Ag nanoparticles *in situ* formed on the surfaces of AgBr and Ag_3PO_4 particles during the photocatalytic reaction.

1. Introduction

For solving many environmental and energy issues, semiconductor-based photocatalysis is taken as a promising avenue [1–3]. In order to highly utilize the solar energy, developing efficient visible-light-driven photocatalysts (such as BiOX (X = Br, I) [4–7], Bi_2WO_6 [8,9], $BiVO_4$ [9,10], $Ag_2Mo_4O_{13}$ [11] and $Ca_xZn_{(1-x)}N_xO_{(1-x)}$ solid solutions [12], *etc.*) consequently has become an imperative topic in current photocatalysis field.

Lately, as nonmetallic p-block elements, P or C elements were incorporated into a simple oxide of narrow band gap (Ag_2O), which has been used as a strategy to design new visible-light-driven photocatalysts, such as Ag_3PO_4 [13] and Ag_2CO_3 [14]. The Ag_3PO_4 (indirect band gap of 2.36 eV as well as a direct band gap of 2.43 eV) [13,15] has been recognized as one of the most efficient visible-light-driven photocatalysts because of its excellent photooxidative capabilities for organic dye decomposition and O_2 evolution from water under visible light irradiation [13]. Through controlling particle size [16], shape and facet effects [17] of Ag_3PO_4 crystals, the photocatalytic activity of Ag_3PO_4 can be further enhanced. However, the unwanted and uncontrolled photodecomposition by light and the low structural stability in water of Ag_3PO_4 decreased the photocatalytic activity during the photocatalytic reaction, which inevitably become a main obstacle for Ag_3PO_4 in practical application.

In recent years, Ye and co-workers [18] have reported that the AgX/Ag_3PO_4 (X = Cl, Br, I) heterocrystals prepared by *in situ* ion-exchange method embodied some advantages compared to the single Ag_3PO_4. Firstly, the insoluble AgX nanoparticles could effectively inhibit the dissolution of Ag_3PO_4 in aqueous solutions [18]. Secondly, AgX and Ag_3PO_4 had matching band potentials, which facilitated the fast transfer and separation of the photoinduced carriers. Thus, AgX/Ag_3PO_4 (X = Cl, Br, I) system is a more promising and fascinating visible-light-driven photocatalyst than pure Ag_3PO_4.

It is well known that silver-based compounds, such as AgX, Ag_3PO_4, Ag_2CO_3 and Ag_2MoO_4, are easily decomposed to generate metal Ag after light irradiation. For example, Ag@AgX [19–24] have been used as highly efficient plasmonic photocatalysts that have Ag nanoparticles (NPs) deposited directly onto the surface of AgX particles via UV or visible light irradiation. Noble Ag NPs, as well as other noble metal NPs (Au, Pt and Pd), can dramatically amplify the absorption of visible light (surface plasmon resonance (SPR) effect [24–26]) and efficiently trap photoinduced electrons [27,28]. However, no attention has been paid to the Ag NPs formed in the AgX/Ag_3PO_4 system. What a special role does it play in the AgX/Ag_3PO_4 system? Furthermore, it is very important to illustrate the mechanism of activity enhancement for AgX/Ag_3PO_4 system clearly, including the generation and separation of the photoinduced carriers, roles of Ag NPs, and the main reactive oxygen species involved in photocatalytic reaction.

* Corresponding author. Tel.: +86 561 3806611; fax: +86 561 3803141.
E-mail addresses: caojing@mail.ipc.ac.cn (J. Cao), chshifu@chnu.edu.cn (S. Chen).

0304-3894/$ – see front matter © 2012 Elsevier B.V. All rights reserved.
doi:10.1016/j.jhazmat.2012.03.002

Herein, we report a newly constructed $AgBr/Ag_3PO_4$ hybrid with different AgBr contents by *in situ* anion-exchange method. $AgBr/Ag_3PO_4$ can easily transform to be $Ag@AgBr/Ag_3PO_4@Ag$ system in the early stage of the photocatalytic reaction. This novel composite system ($AgBr/Ag_3PO_4$, Ag@AgBr and $Ag@Ag_3PO_4$) is highly expected to exhibit excellent photocatalytic activity. Methyl orange (MO) and phenol were used as model pollutants to evaluate the photocatalytic activity of the $AgBr/Ag_3PO_4$ hybrid under visible light ($\lambda > 420$ nm). Based on the results of the repetition tests, the different roles of Ag NPs on the activity and stability of the photocatalyst was investigated. Additionally, various scavengers were introduced to the photocatalytic reaction system to explore the effects of different reactive oxygen species in the MO degradation process.

2. Experimental

2.1. Chemicals and materials

All reagents were of analytical purity and were used without further purification. Silver nitrate ($AgNO_3$), sodium bromide (NaBr), sodium dihydrogen phosphate dihydrate ($NaH_2PO_4{\cdot}2H_2O$), methyl orange, phenol, terephthalic acid (TA), benzoquinone (BQ), ammonium oxalate (AO), tert-butyl alcohol (TBA), catalase (CAT), and sodium hydroxide (NaOH) were obtained from Sinopharm Chemical Reagent Co., Ltd. Deionized water was used throughout this study.

2.2. Preparation of $AgBr/Ag_3PO_4$ photocatalyst

The synthesis of Ag_3PO_4 precursor was achieved by a simple precipitation reaction in a dark condition at room temperature. In a typical procedure, 5.59 g of $NaH_2PO_4{\cdot}2H_2O$ and 18.27 g of $AgNO_3$ were dissolved in deionized water in advance, respectively, then dilute NaOH solution (0.1 M) was dropped into NaH_2PO_4 solution to adjust the pH value of the solution to 8.50 with stirring. Subsequently, while $AgNO_3$ solution was added dropwise into above solution, the pH of the suspension was kept at 8.00 using NaOH solution (0.1 M). After vigorously stirring for 5 h, the yellow precipitate was collected, rinsed with deionized water for 3 times, and dried at 60 °C for 24 h to obtain Ag_3PO_4.

$AgBr/Ag_3PO_4$ was prepared through an *in situ* anion-exchange method in a dark condition at room temperature. Initially, 1.0 g of Ag_3PO_4 was dispersed in 50 mL of deionized water and then the suspension was sonicated for 30 min. Subsequently, different stoichiometric amounts of NaBr solution were added slowly into above suspension with constant stirring. After addition, the mixtures were vigorously stirring for 3 h. The theoretical molar percentages of added Br/original P were controlled to be 20%, 40%, 60% and 80%, respectively. Finally, the precipitates were collected, washed with deionized water for 3 times, and dried at 60 °C for 24 h. The final samples were denoted as 20% $AgBr/Ag_3PO_4$, 40% $AgBr/Ag_3PO_4$, 60% $AgBr/Ag_3PO_4$ and 80% $AgBr/Ag_3PO_4$, respectively.

For comparison, pure AgBr sample was also prepared by a simple precipitation method according to our previous study [29].

2.3. Characterization of $AgBr/Ag_3PO_4$ photocatalyst

XRD analysis of the as-prepared samples was carried out at room temperature with a Bruker D8 Advance X-diffractometer using Cu Kα radiation ($\lambda = 1.5406$ Å), operated at 40 kV and 40 mA, and a scanning speed of 10°/min. XPS measurements were performed on a Thermo ESCALAB 250 with Al Kα (1486.6 eV) line at 150 W. To compensate for surface charges effects, binding energies were calibrated using the C1s peak at 284.80 eV as the reference. FE-SEM measurements were recorded on a FEI Sirion200 with an accelerating voltage of 5.00 kV. Energy-dispersive spectroscopy (EDS) was observed by using an Oxford instruments INCA X-act detector. The DRS were obtained by a Pgeneral TU-1901 UV–VIS spectrophotometer equipped with an integrating sphere assembly. The analysis range was from 300 to 800 nm, and $BaSO_4$ was used as a reflectance standard. Fluorescence emission spectra were recorded on a JASCO FP-6500 type fluorescence spectrophotometer with 260 nm excitation source over a wavelength range of 400–650 nm. Shimadzu TOC-V_{CPH} total organic carbon analyzer was used to detect the total organic carbon (TOC) of MO and phenol solution.

2.4. Photocatalytic activities test

The photodegradation of MO was adopted to evaluate the photocatalytic activity of $AgBr/Ag_3PO_4$ in a photoreaction apparatus [29]. A 500 W Xe lamp (Institute of Electric Light Source, Beijing) was used as the light source with a 420 nm cutoff filter (Instrument Company of Nantong, China) to provide visible-light irradiation. In each experiment, 0.10 g photocatalyst was added into 50 mL of MO solution (10 mg L^{-1}). Prior to illumination, the suspension was magnetically stirred in the dark for 30 min to reach adsorption–desorption equilibrium of MO on catalyst surfaces. At irradiation time intervals of 10 min, 5 mL of the suspension was collected, then centrifuged (4000 rpm, 30 min) and filtered through 0.22 μm millipore filter to remove the photocatalyst particles. The catalyst-free dye solution was analyzed with a 722 s spectrophotometer (Shanghai Youke Instrument Co., Ltd., China). The concentration of MO was determined from its maximum absorption at a wavelength of 464 nm with deionized water as a reference sample.

In addition, the degradation of phenol aqueous solution over 60% $AgBr/Ag_3PO_4$ under visible light ($\lambda > 420$ nm) was also carried out (see Supplementary Data).

The TOC values of degradation of MO and phenol solution over 60% $AgBr/Ag_3PO_4$ were detected, respectively, by a Shimadzu TOC-V_{CPH} total organic carbon analyzer to determine the extent of mineralization.

2.5. Detection of reactive oxygen species

The examination experiment process of reactive oxygen species is similar to the photodegradation experiment. Different quantity of scavengers was introduced into the MO solution prior to addition of the catalyst. The dosages of these scavengers were referred to the previous studies [30–32].

In addition, photoluminescence (PL) technique with terephthalic acid as a probe molecule was used to investigate the formation of $^{\bullet}OH$ radicals [33,34] on the surface of $AgBr/Ag_3PO_4$ illuminated by visible light irradiation. The experimental procedures were carried out according to our previous studies [35].

3. Results and discussion

3.1. XRD and XPS analysis

Fig. 1 shows the XRD patterns of the as-prepared samples. It is observed that Ag_3PO_4 (Fig. 1a) was cubic phase (JCPDS NO. 06-0505) while AgBr (Fig. 1f) was face-centered cubic AgBr structure (JCPDS NO. 06-0438). In addition, the $AgBr/Ag_3PO_4$ hybrid (Fig. 1b–e) exhibited a coexistence of both AgBr and Ag_3PO_4 phases. With increasing AgBr content, the intensities of diffraction peaks of AgBr increased whereas those of Ag_3PO_4 decreased simultaneously. Furthermore, all the used $AgBr/Ag_3PO_4$ hybrids became a little darker than the corresponding fresh $AgBr/Ag_3PO_4$ hybrids. For instance, the diffraction peaks at 38.07° (JCPDS NO. 04-0783) assigned to Ag were displayed in the used 60% $AgBr/Ag_3PO_4$ after 1

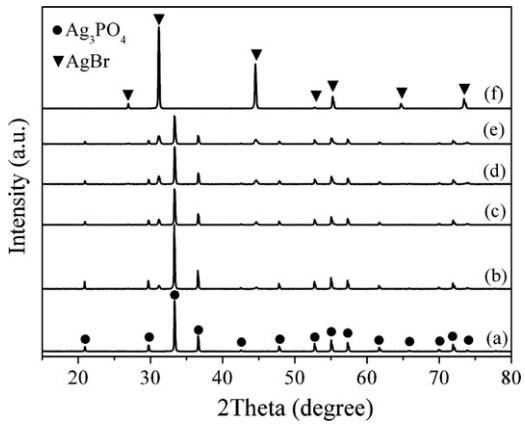

Fig. 1. XRD patterns of (a) Ag_3PO_4, (b) 20% $AgBr/Ag_3PO_4$, (c) 40% $AgBr/Ag_3PO_4$, (d) 60% $AgBr/Ag_3PO_4$, (e) 80% $AgBr/Ag_3PO_4$ and (f) AgBr.

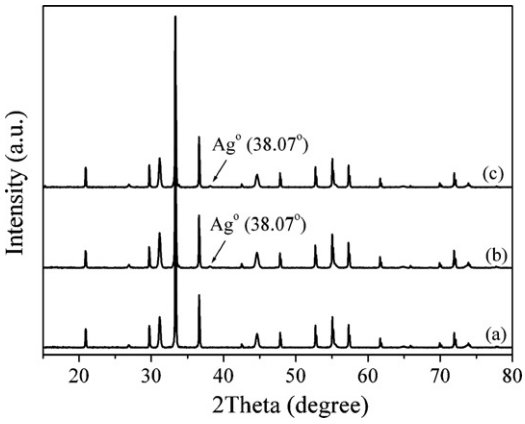

Fig. 2. XRD patterns of (a) the fresh 60% $AgBr/Ag_3PO_4$, (b) the used 60% $AgBr/Ag_3PO_4$ after 1 recycling run and (d) the used 60% $AgBr/Ag_3PO_4$ after 5 recycling runs.

(Fig. 2b) and 5 (Fig. 2c) recycling runs compared with the fresh 60% $AgBr/Ag_3PO_4$ (Fig. 2a), whereas the crystal structures of both AgBr and Ag_3PO_4 were still well maintained.

In addition, the appearance of metal Ag in the used $AgBr/Ag_3PO_4$ hybrids can be further confirmed by the XPS. The surface element composition and chemical state for the used 60% $AgBr/Ag_3PO_4$ were analyzed by XPS and the results are shown in Figs. 3 and 4. The binding energies of the XPS spectra were calibrated by C1s (284.8 eV). The Ag 3d spectra of the used 60% $AgBr/Ag_3PO_4$ after 1 (Fig. 3a) and

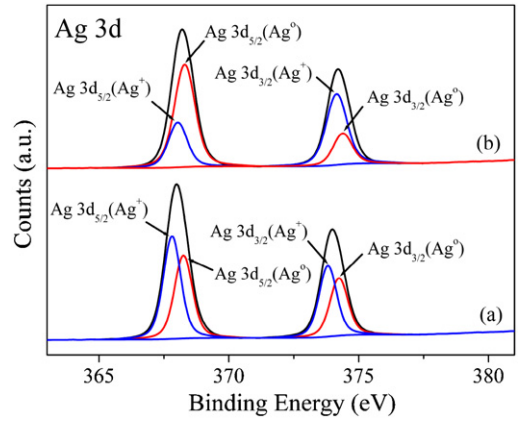

Fig. 3. Ag 3d XPS spectra of (a) the used 60% $AgBr/Ag_3PO_4$ after 1 recycling run and (b) the used 60% $AgBr/Ag_3PO_4$ after 5 recycling runs.

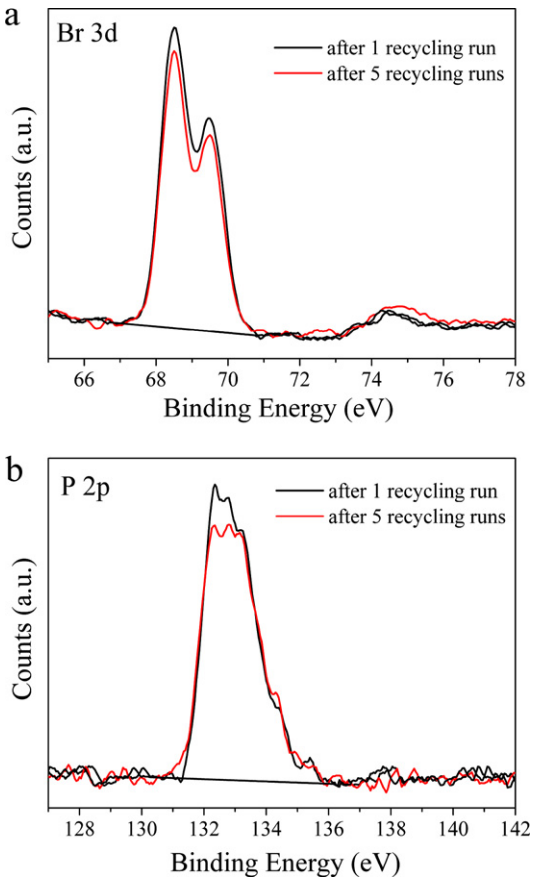

Fig. 4. (a) Br 3d and (b) P 2p XPS spectra of the used 60% $AgBr/Ag_3PO_4$ (black line: after 1 recycling run; red line: after 5 recycling runs). (For interpretation of the references to color in this figure legend, the reader is referred to the web version of the article.)

5 (Fig. 3b) recycling runs are shown in Fig. 3. The Ag 3d peaks of the used $AgBr/Ag_3PO_4$ hybrids were consisted of two individual peaks, corresponding to Ag and Ag^+, respectively. According to Zhang et al. [36], the peaks at 368.25 and 374.24 eV can be attributed to Ag, whereas the peaks at 367.81 and 373.81 eV can be attributed to the Ag^+ of AgBr and Ag_3PO_4. It clearly shows that the intensity of Ag^+ decreased while that of Ag increased during the photocatalytic process, which indicates that partial Ag^+ gradually transformed to be metal Ag under the sustaining irradiation. The decrease in intensity of Br 3d (Fig. 4a) and P 2p (Fig. 4b) XPS spectra of the used 60% $AgBr/Ag_3PO_4$ from 1 to 5 recycling runs also proved that the amount of Ag has become larger. The detailed contents of all the elements in $AgBr/Ag_3PO_4$ hybrids are displayed in Table 1. These results suggest that $AgBr/Ag_3PO_4$ has transformed to be $Ag@AgBr/Ag_3PO_4@Ag$ composite photocatalyst after light irradiation during the photocatalytic process without additional light reduction treatment before the photocatalysis.

3.2. FE-SEM and EDS analysis

The FE-SEM images of Ag_3PO_4 and $AgBr/Ag_3PO_4$ hybrids are presented in Fig. 5, and the corresponding EDS results are shown as insets. Fig. 5a displays that Ag_3PO_4 particles had irregular shapes with size of about 0.2–0.8 μm. The particle size and morphology of the $AgBr/Ag_3PO_4$ hybrids (Fig. 5b–e) were approximately similar to that of Ag_3PO_4, except for some smaller AgBr particles formed. Because it is not clear to distinguish between $AgBr/Ag_3PO_4$ hybrids and Ag_3PO_4, the EDS of them were necessary. It presents that pure Ag_3PO_4 were composed of Ag, P and O elements, whereas

Table 1
XPS results of the used 60% $AgBr/Ag_3PO_4$.

Catalyst	XPS results (at.%)					
	Ag^+	Ag	Br	P	O	C
60% $AgBr/Ag_3PO_4$ after 1 recycling run	13.18	10.93	4.58	5.13	35.03	31.15
60% $AgBr/Ag_3PO_4$ after 5 recycling runs	5.96	15.00	4.03	5.02	39.09	30.90

$AgBr/Ag_3PO_4$ were consisted of Ag, P, Br and O elements, which further proves that AgBr existed in all the $AgBr/Ag_3PO_4$ hybrids. In addition, no other impurity was appeared in the system. The change tendency of AgBr contents obtained from EDS results were agreed with the XRD data. Therefore, the as-prepared samples had similar morphologies but had different components from each other.

3.3. DRS analysis

Fig. 6a shows the DRS of the AgBr, Ag_3PO_4 and $AgBr/Ag_3PO_4$ hybrids. As can be seen, AgBr had an absorption edge at about 480 nm, while Ag_3PO_4 had broader absorption in the visible region with an absorption edge of around 530 nm [13]. The $AgBr/Ag_3PO_4$ exhibited a mixed absorption property of AgBr and Ag_3PO_4. In the wavelength range from 400 to 500 nm, with increasing AgBr content, the absorption edge of $AgBr/Ag_3PO_4$ had a weak blue shift compared to single Ag_3PO_4. Differently, the used 60% $AgBr/Ag_3PO_4$ after 1 and 5 recycling runs had much stronger absorption in the visible region than that of the fresh 60% $AgBr/Ag_3PO_4$, as shown in Fig. 6b, which may result from the strong SPR effect of Ag NPs deposited on the AgBr and Ag_3PO_4 particles [19–24,37]. Furthermore, the absorption in the visible region was enhanced from 1 to

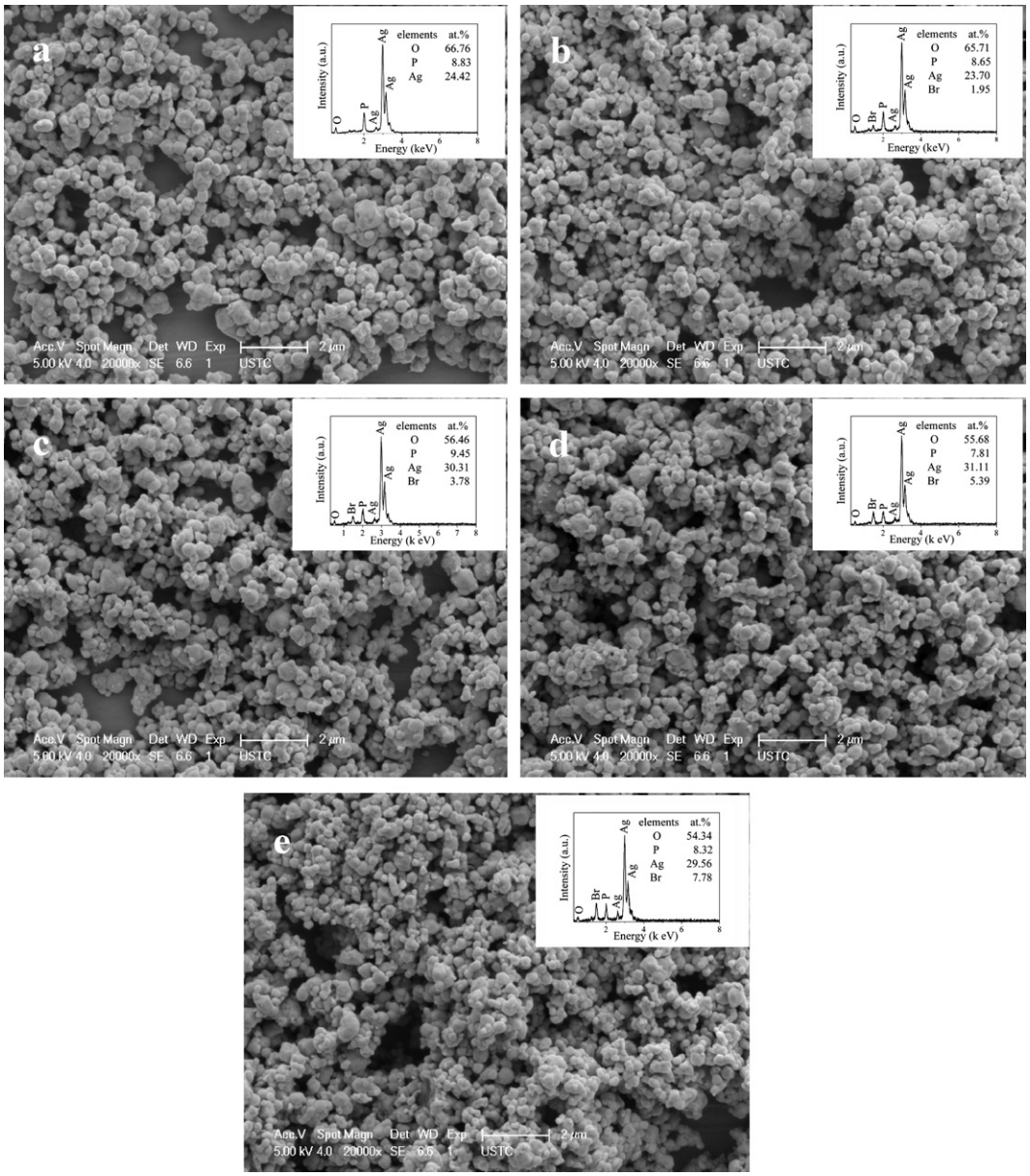

Fig. 5. FE-SEM images of (a) Ag_3PO_4, (b) 20% $AgBr/Ag_3PO_4$, (c) 40% $AgBr/Ag_3PO_4$, (d) 60% $AgBr/Ag_3PO_4$ and (e) 80% $AgBr/Ag_3PO_4$ (insets show the corresponding EDS).

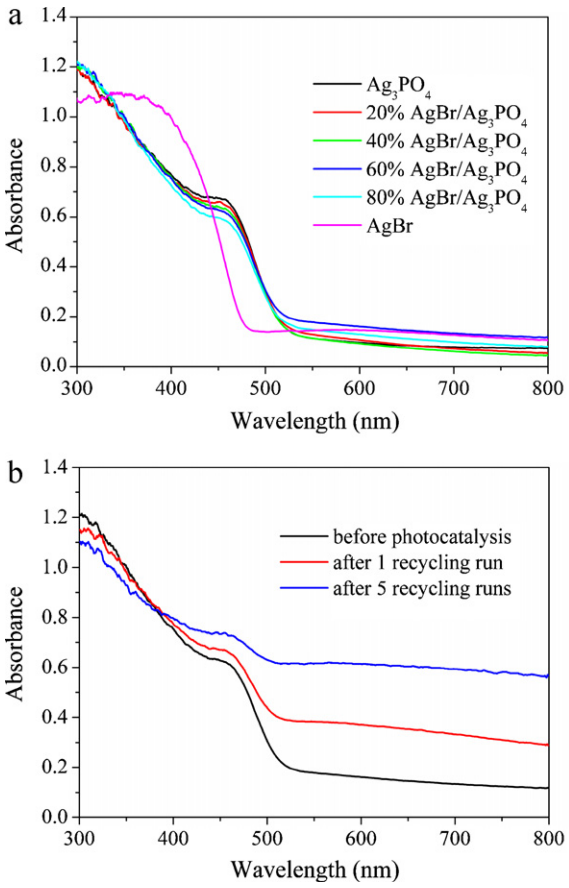

Fig. 6. (a) DRS of AgBr, Ag_3PO_4 and $AgBr/Ag_3PO_4$ hybrids. (b) DRS of the fresh 60% $AgBr/Ag_3PO_4$ (black line), the used 60% $AgBr/Ag_3PO_4$ after 1 recycling run (red line) and the used 60% $AgBr/Ag_3PO_4$ after 5 recycling runs (blue line). (For interpretation of the references to color in this figure legend, the reader is referred to the web version of the article.)

5 recycling runs, indicating that the amount of metal Ag increased in the photocatalytic reaction, which is consistent with the XPS data (Fig. 3). The increased content of metal Ag will affect the size of Ag, which further affects the separation of photoinduced carriers [38], the SPR effect of Ag NPs [20,39] and then corresponding photocatalytic activities. Further discussion will be carried out to discuss the stability of $AgBr/Ag_3PO_4$ hybrids.

In order to further confirm the position of metal Ag, the XRD and DRS experiments of single Ag_3PO_4 and AgBr before and after photocatalysis were adapted, respectively, as shown in Fig. S1–S2. The results show that metal Ag can be formed on the surface of Ag_3PO_4 [37] as well as AgBr [23,24], which means that $AgBr/Ag_3PO_4$ hybrid has converted to $Ag@AgBr/Ag_3PO_4@Ag$ system during the photocatalytic reaction process.

The band gap energy of a semiconductor can be calculated by the following formula [40]:

$$\alpha h\nu = A(h\nu - E_g)^{n/2} \quad (1)$$

where α, h, ν, E_g and A are absorption coefficient, Planck constant, light frequency, band gap energy, and a constant, respectively. Among them, n is determined from the type of optical transition of a semiconductor ($n = 1$ for direct transition and $n = 4$ for indirect transition). For AgBr and Ag_3PO_4, the values of n are 4 [41] and 1 [13], respectively. Therefore, E_g of AgBr was determined from a plot of $(\alpha h\nu)^{1/2}$ *versus* energy ($h\nu$) (Fig. 7) and was elicited to be 2.46 eV. Accordingly, E_g of Ag_3PO_4 was found to be 2.45 eV according to a plot of $(\alpha h\nu)^2$ *versus* energy ($h\nu$) (Fig. 7).

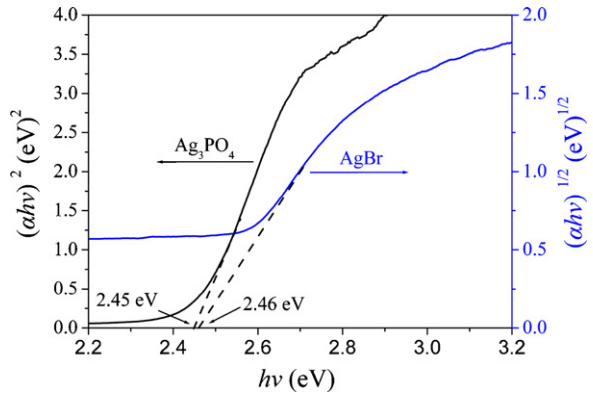

Fig. 7. Plot of $(\alpha h\nu)^{1/2}$ *versus* energy ($h\nu$) for the band gap energy of AgBr and the plot of $(\alpha h\nu)^2$ *versus* energy ($h\nu$) for the band gap energy of Ag_3PO_4.

In addition, the valence band (VB) edge positions of AgBr and Ag_3PO_4 components were estimated according to the concept of electronegativity. Herein, the electronegativity of an atom is the arithmetic mean of the atomic electron affinity and the first ionization energy. The VB edge potential of a semiconductor at the point of zero charge can be calculated by the following empirical equation [42]:

$$E_{VB} = X - E^c + 0.5E_g \quad (2)$$

where E_{VB} is the VB edge potential, X is the electronegativity of the semiconductor, which is the geometric mean of the electronegativity of the constituent atoms, E^c is the energy of free electrons on the hydrogen scale (about 4.5 eV), E_g is the band gap energy of the semiconductor. Moreover, conduction band (CB) edge potential (E_{CB}) can be determined by $E_{CB} = E_{VB} - E_g$. The X values for AgBr and Ag_3PO_4 are 5.81 and 5.96 eV, and the E_{VB} of AgBr and Ag_3PO_4 were calculated to be 2.54 and 2.69 eV/NHE, respectively. Thus, the E_{CB} of AgBr and Ag_3PO_4 were estimated to be 0.08 and 0.24 eV/NHE, respectively.

3.4. Degradation of MO using $AgBr/Ag_3PO_4$ photocatalyst

The photocatalytic activities of as-prepared samples were evaluated by the degradation of MO under visible light ($\lambda > 420$ nm). Fig. 8a displays the photodegradation of MO as a function of irradiation time over different photocatalysts. From the blank (in the absence of any catalyst) and the dark (without irradiation) experiments, the self-photolysis of MO upon visible light irradiation and the dark adsorption of MO over each sample can be neglected, as shown in Fig. 8a. All the $AgBr/Ag_3PO_4$ hybrids exhibited higher photocatalytic activities than pure Ag_3PO_4. As the AgBr content increased to 60%, the highest photocatalytic activity was achieved, at which 95.1% of MO was decomposed after 50 min irradiation. However, the photocatalytic activity decreased when the AgBr content rose to 80%. These results suggest that the optimal AgBr content in $AgBr/Ag_3PO_4$ existed when the Br/P molar ratio was 0.60.

Moreover, Fig. 8b clearly shows that the photocatalytic activity of 60% $AgBr/Ag_3PO_4$ (100 mg) is much higher than that of mathematical sum of AgBr (25.2 mg) and Ag_3PO_4 (74.8 mg), in which they contain the same weight of visible-light-active components as in 60% $AgBr/Ag_3PO_4$. It is resulted from the decrease in recombination rate of electron–hole pairs, which can be attributed to the heterojunction between AgBr and Ag_3PO_4 formed in $AgBr/Ag_3PO_4$ hybrid.

Since MO can absorb visible light, the sensitization possibility for $AgBr/Ag_3PO_4$ hybrid should be considered. In order to ensure the photocatalytic activity of $AgBr/Ag_3PO_4$ hybrid and exclude the dye sensitization under visible light, degradation of a

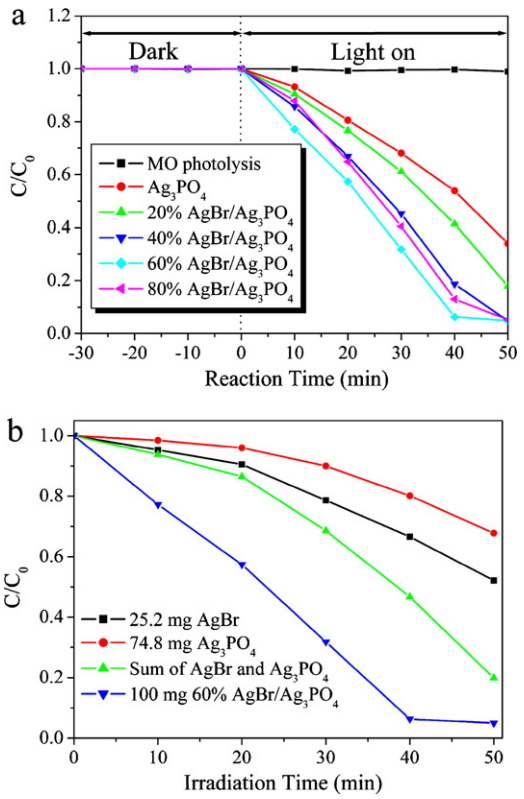

Fig. 8. (a) Photocatalytic activities of Ag_3PO_4 and $AgBr/Ag_3PO_4$ hybrids on the degradation of MO under visible light ($\lambda > 420$ nm). (b) Comparison of photocatalytic activities of different photocatalysts with the same weight of each visible-light-active component: 25.2 mg AgBr (black line), 74.8 mg Ag_3PO_4 (red line), mathematical sum of 25.2 mg AgBr and 74.8 mg Ag_3PO_4 (green line), and 100.00 mg 60% $AgBr/Ag_3PO_4$ containing 25.2 mg AgBr and 74.8 mg Ag_3PO_4 (blue line) on the degradation of MO under visible light. (For interpretation of the references to color in this figure legend, the reader is referred to the web version of the article.)

typical colorless organic contaminant is a better choice. Therefore, phenol was chosen as another moderate contaminant to further estimate the photocatalytic performance in our study, and the results are shown in Fig. S3. It displays that the peak intensity of phenol at 270 nm decreased obviously with increasing irradiation time, indicating that phenol can be effectively degraded over 60% $AgBr/Ag_3PO_4$ under visible light. Because colorless phenol cannot sensitize $AgBr/Ag_3PO_4$, this can be used as a forceful proof to ensure the photocatalytic activity of $AgBr/Ag_3PO_4$.

The TOC experiments of MO and phenol solution in the presence of 60% $AgBr/Ag_3PO_4$ were also performed, respectively. For MO solution, the TOC of MO solution decreased by *ca.* 51.8% after irradiation for 50 min, suggesting that MO had not only been decolorized but also mineralized over $AgBr/Ag_3PO_4$ hybrid under visible irradiation. However, the rate of TOC reduction is slower than that of the degradation of MO which is nearly 100% discoloration for MO in 40 min, as shown in Fig. 8a, suggesting that MO may be first partial degradation to colorless products and then converted into CO_2 in the photocatalytic reaction process [43,44]. For phenol solution, as depicted in Fig. S4, the TOC values of phenol solution decreased gradually with increasing irradiation time and the phenol mineralization degree reached a value of 82.5% after 100 min of irradiation.

3.5. Stability of $AgBr/Ag_3PO_4$ photocatalyst

To evaluate the stability of $AgBr/Ag_3PO_4$ hybrid, we conducted the repeatability experiments of MO degradation over 60% $AgBr/Ag_3PO_4$ and the result is shown in Fig. 9. After 4 recycling runs

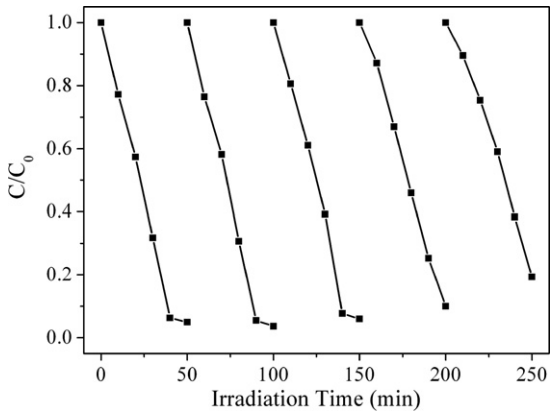

Fig. 9. Cycling runs of 60% $AgBr/Ag_3PO_4$ for the degradation of MO under visible light irradiation.

for the photodegradation of MO, the high photocatalytic performance of $AgBr/Ag_3PO_4$ was effectively maintained except for 5.1% decrease in photocatalytic efficiency, suggesting that $AgBr/Ag_3PO_4$ has high stability under visible light. This result indicates that though $AgBr/Ag_3PO_4$ is not stable in the initial reaction process under visible light, the formed Ag@$AgBr/Ag_3PO_4$@Ag plasmonic system can effectively retain its activity due to the efficient transfer of photoinduced electrons. Special mention must be made, the photocatalytic activity decreased obviously, down to 80.7% of MO degradation after 5 recycling runs. In order to understand this phenomenon, the roles of Ag NPs controlled by their sizes should be addressed.

3.6. Possible photocatalytic mechanism

3.6.1. Fluorescence emission spectra

In a photocatalytic reaction, the activity is largely affected by the recombination of the photoinduced electrons and holes, which will decrease the quantum yield [45]. It is known that the recombination of electron–hole pairs can release energy in the form of fluorescence emission. Lower fluorescence emission intensity implies lower electron–hole recombination rate and corresponds to higher photocatalytic activity [46].

Using an ultraviolet light with a 260 nm wavelength as excitation source, the fluorescence emission spectra of AgBr, Ag_3PO_4 and $AgBr/Ag_3PO_4$ hybrids are presented in Fig. 10. It can be seen that both AgBr and Ag_3PO_4 show higher intensity of emission spectra than those of all the $AgBr/Ag_3PO_4$ hybrids. In case of pure AgBr and Ag_3PO_4, the photoinduced electrons and holes might recombine

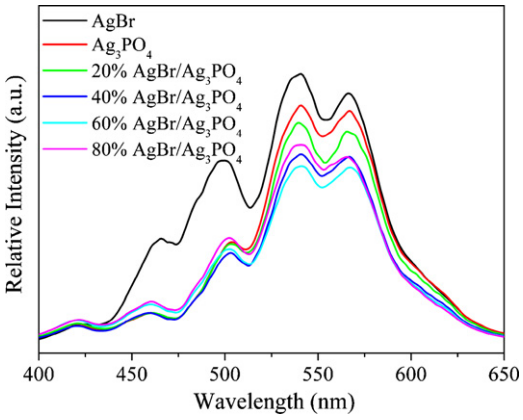

Fig. 10. Fluorescence emission spectra of AgBr, Ag_3PO_4 and $AgBr/Ag_3PO_4$ hybrids.

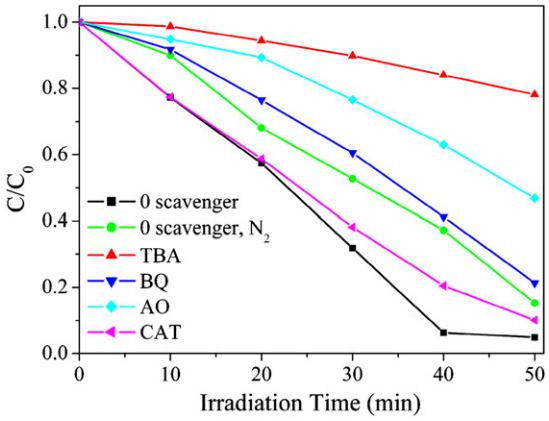

Fig. 11. Effects of different scavengers on degradation of MO in the presence of 60% $AgBr/Ag_3PO_4$ and under N_2-saturated condition.

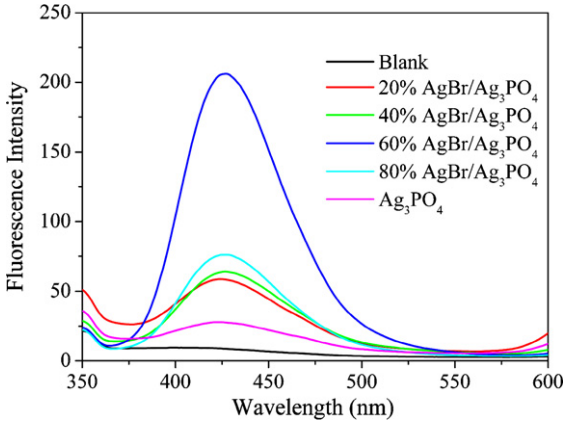

Fig. 12. PL spectra of Ag_3PO_4 and $AgBr/Ag_3PO_4$ hybrids in TA solution (each sample was illuminated for 20 min of visible light).

rapidly because of their narrow band gaps. However, in the case of $AgBr/Ag_3PO_4$ hybrids, the photoinduced carriers can migrate easily between AgBr and Ag_3PO_4 due to their matching band potentials and therefore the electron–hole recombination rate is greatly decreased. This result shows that $AgBr/Ag_3PO_4$ heterojunction is helpful to inhibit the recombination of photoinduced carriers and improve the corresponding photocatalytic activity.

In addition, the emission intensity of $AgBr/Ag_3PO_4$ decreased from 20% to 60% $AgBr/Ag_3PO_4$, and then increased up to 80% $AgBr/Ag_3PO_4$, in which 60% $AgBr/Ag_3PO_4$ displayed the lowest intensity of emission spectra. It indicates that 60% $AgBr/Ag_3PO_4$ has the lowest electron–hole recombination rate, suggesting that the electrons and holes have longer lifetime and may form more amount of reactive species. This coincides with the highest photocatalytic activity of 60% $AgBr/Ag_3PO_4$. $AgBr/Ag_3PO_4$ photocatalysts with other AgBr contents had correspondingly lower photocatalytic activity than 60% $AgBr/Ag_3PO_4$.

3.6.2. Roles of reactive oxygen species

It is generally accepted that the dyes and organic pollutants can be photodegraded via photocatalytic oxidation (PCO) process. A large number of main reactive oxygen species (ROSs) including h^+, H_2O_2, $^\bullet OH$ and $^\bullet O_2^-$ involved in PCO process [32,47,48]. Therefore, the effects of some scavengers and N_2 purging without adding any scavengers on the degradation of MO were examined in attempt to elucidate the reaction mechanism. In this study, TBA was added to the reaction system as an $^\bullet OH$ scavenger [32,49], and AO was introduced as a scavenger of h^+ [31,50,51]. BQ was adopted to quench $^\bullet O_2^-$ [52,53], and CAT was used as a H_2O_2 scavenger [30].

Fig. 11 shows that in the presence of TBA or AO, the photodegradation of MO was inhibited significantly compared with no scavenger at the same conditions, indicating the main roles of $^\bullet OH$ and h^+ for MO degradation. The addition of BQ and CAT showed weaker effects in PCO process of MO, suggesting that $^\bullet O_2^-$ and H_2O_2 played comparatively minor role for MO degradation.

In order to further confirm the existence of $^\bullet OH$, the formed $^\bullet OH$ on the surface of $AgBr/Ag_3PO_4$ hybrids illuminated by visible light were detected by PL technique. The experimental conditions were the same as the photocatalytic reaction system. The PL emission spectra excited at 315 nm from TA solution suspension with different $AgBr/Ag_3PO_4$ hybrids and Ag_3PO_4 were measured after each sample was illuminated for 20 min of visible light. Fig. 12 displays that a PL signal was observed at 425 nm for each $AgBr/Ag_3PO_4$ hybrid. The PL intensity was enhanced to maximum (60% $AgBr/Ag_3PO_4$) and then declined with increasing AgBr content. This suggests that the fluorescence is caused by chemical reactions of TA with $^\bullet OH$ formed in photocatalytic reactions [33,34]. Hence, $^\bullet OH$ is the reactive oxygen species in $AgBr/Ag_3PO_4$ system and finally induces the degradation of MO. Moreover, 60% $AgBr/Ag_3PO_4$ with maximal photocatalytic activity produced much more reactive $^\bullet OH$ than other samples, which is also consonant with the results of fluorescence emission spectra (Fig. 10).

Furthermore, all the $AgBr/Ag_3PO_4$ hybrids show higher PL intensity than pure Ag_3PO_4, suggesting that *in situ* loading AgBr on the surface of Ag_3PO_4 particles is a good way to accelerate the transfer and separation of the photoinduced carriers, which leads to the increase of $^\bullet OH$ formation.

Because of the lower E_{CB} values of Ag_3PO_4 and AgBr, both Ag_3PO_4 and AgBr can not provide a sufficient potential to reduce O_2 to $^\bullet O_2^-$ ($E^\circ(O_2/^\bullet O_2^-) = -0.33$ V/NHE) [49,54] through the one-electron reduction process and further generate $^\bullet OH$. Therefore, it is reasonable for O_2 to combine with electrons trapped by noble Ag NPs and form H_2O_2 (Eq. (3)) via a two-electron reduction reaction process [18,49,55–57] ($E^\circ(O_2/H_2O_2) = +0.695$ V/NHE) [49]. Then the formed H_2O_2 quickly reacts with an electron to finally generate $^\bullet OH$ (Eq. (4)).

$$O_2 + 2H^+ + 2e^- \rightarrow H_2O_2 \quad (3)$$

$$H_2O_2 + e^- \rightarrow {}^\bullet OH + OH^- \quad (4)$$

On the other hand, experiments with purging N_2 were carried out to examine the role of dissolved O_2. As can be seen from Fig. 11, when N_2 purging (0 scavenger) was conducted, the degradation of MO was decreased compared with air-equilibrated conditions (0 scavenger), confirming that the dissolved O_2 can primarily act as an efficient electrons trap, leading to the generation of $^\bullet OH$, and simultaneously preventing the recombination of electrons and holes [32,48].

In addition, reactive holes at the VB top of AgBr will oxidize MO directly due to its insufficient potential to oxidize surface adsorbed H_2O to $^\bullet OH$ ($E^\circ(^\bullet OH, H^+/H_2O) = 2.72$ V/NHE) [30].

3.6.3. Possible degradation mechanism and the role of Ag nanoparticles

On the base of band gap structure of $AgBr/Ag_3PO_4$ and the effects of scavengers, a possible pathway for the photodegradation of MO with $AgBr/Ag_3PO_4$ photocatalyst was proposed as follows (Fig. 13):

During the PCO process, the $AgBr/Ag_3PO_4$ system was transformed to be $Ag@AgBr/Ag_3PO_4@Ag$ system. Ag_3PO_4 and AgBr can be simultaneously excited to form electron–hole pairs under visible light irradiation. On the one hand, the photoinduced electrons transfer from the CB bottom of AgBr to that of Ag_3PO_4 and then are trapped by Ag NPs through path (1) in Fig. 13. On the other hand, the photoinduced electrons on the CB bottom of AgBr can also be

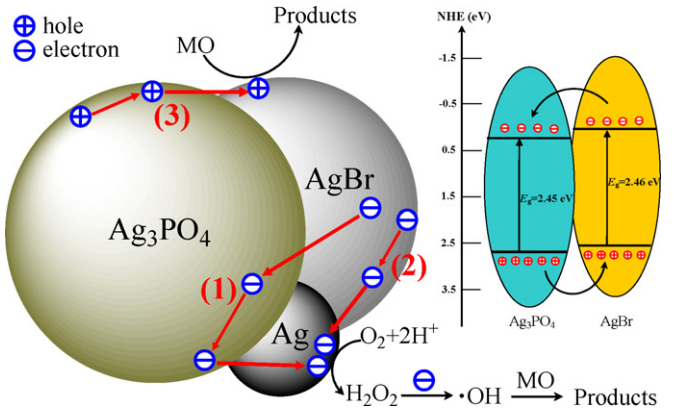

Fig. 13. Schematic diagram of electron–hole pairs separation and the possible reaction mechanism over Ag@AgBr/Ag_3PO_4@Ag photocatalyst under visible light irradiation. (Only the Ag NPs contact with both Ag_3PO_4 and AgBr particles is displayed here.)

trapped by Ag NPs directly through path (2) in Fig. 13. At the same time, the photogenerated holes also move in the opposite direction from the VB top of Ag_3PO_4 to that of AgBr through path (3) in Fig. 13. These photoinduced electrons trapped by Ag NPs will further react with the O_2 via two-electron reduction process (Eq. (3)) to finally generate reactive •OH (Eq. (4)) that will induce the degradation of MO. Meanwhile, reactive holes at the VB of AgBr will oxidize MO directly. Through this way, the photogenerated carriers can be separated efficiently and improved the photocatalytic activities of AgBr/Ag_3PO_4.

In addition, as mentioned above, the decrease in the photocatalytic activity has been observed during the cycle experiments, as shown in Fig. 9, which may be mainly controlled by the Ag NPs that can display different roles in the photocatalytic reaction due to the changes in the size of Ag_n clusters [38].

(1) *For small n*, the photoinduced electron can be effectively trapped by the small Ag NPs [27,58–60] deposited on the surface of AgBr and Ag_3PO_4 with the effect of decreasing recombination of photoinduced carriers, which increases product yields of h^+ and •OH, and further improves the photocatalytic activity of AgBr/Ag_3PO_4.
(2) *For large n*, though the Ag_n cluster still can be used as an electron trap, it is unlikely to transfer electrons to O_2. Besides, the capability of accepting photoinduced holes is enhanced gradually, and thus the Ag_n clusters turn into the combination centers of photoinduced carriers [38,61], which will counteract the activity improvement. Therefore, the changes in the size of Ag_n clusters in the PCO process displayed different roles for the photoinduced carriers, which finally controlled the photocatalytic activity of AgBr/Ag_3PO_4.

In conclusion, the photoinduced electrons and holes can be effectively separated through the *in situ* formed heterojunction of AgBr/Ag_3PO_4 and the trapping role of Ag NPs with limited sizes in the PCO process. Moreover, the SPR effect of Ag NPs ensures enough visible light to be utilized. These are the two main reasons for realizing the activity enhancement of AgBr/Ag_3PO_4 under visible light. This may provide another approach to deeply understand the role of Ag NPs for AgX-based system.

4. Conclusions

The AgBr/Ag_3PO_4 hybrid was synthesized using an *in situ* anion-exchange method. The as-prepared AgBr/Ag_3PO_4 exhibited excellent performance on the degradation of MO and displayed much higher photocatalytic activity than single AgBr or Ag_3PO_4 under visible light ($\lambda > 420$ nm). After 5 cycles of repetition tests, the degradation efficiency of MO still remained 80.7%. Photocatalytic mechanism investigations demonstrate that the degradation of MO over the as-prepared AgBr/Ag_3PO_4 under visible light is mainly via •OH and h^+ oxidation mechanism. The activity changes of AgBr/Ag_3PO_4 depend on not only the heterojunction between AgBr and Ag_3PO_4, but also the Ag NPs controlled by the sizes during the photocatalytic process. It may be a promising efficient composite photocatalyst for environmental purification.

Acknowledgements

This work was financially supported by the Natural Science Foundation of China (No. 20973071, 51172086), the Natural Science Foundation of Educational Committee of Anhui Province (No. 2012Z356) and the youth foundation of Huaibei Normal University (No. 2011xqxm31).

Appendix A. Supplementary data

Supplementary data associated with this article can be found, in the online version, at doi:10.1016/j.jhazmat.2012.03.002.

References

[1] A. Fujishima, K. Honda, Electrochemical photolysis of water at a semiconductor electrode, Nature 238 (1972) 37–38.
[2] M.A. Fox, M.T. Dulay, Heterogeneous photocatalysis, Chem. Rev. 93 (1993) 341–357.
[3] M.R. Hoffmann, S.T. Martin, W. Choi, D.W. Bahnemann, Environmental applications of semiconductor photocatalysis, Chem. Rev. 95 (1995) 69–96.
[4] X. Xiao, W.D. Zhang, Facile synthesis of nanostructured BiOI microspheres with high visible light-induced photocatalytic activity, J. Mater. Chem. 20 (2010) 5866–5870.
[5] Y.Q. Lei, G.H. Wang, S.Y. Song, W.Q. Fan, M. Pang, J.K. Tang, H.J. Zhang, Room temperature, template-free synthesis of BiOI hierarchical structures: visible-light photocatalytic and electrochemical hydrogen storage properties, Dalton Trans. 39 (2010) 3273–3278.
[6] J. Zhang, F.J. Shi, J. Lin, D.F. Chen, J.M. Gao, Z.X. Huang, X.X. Ding, C.C. Tang, Self-assembled 3-D architectures of BiOBr as a visible light-driven photocatalyst, Chem. Mater. 20 (2008) 2937–2941.
[7] M. Shang, W.Z. Wang, L. Zhang, Preparation of BiOBr lamellar structure with high photocatalytic activity by CTAB as Br source and template, J. Hazard. Mater. 167 (2009) 803–809.
[8] L.S. Zhang, H.L. Wang, Z.G. Chen, P.K. Wong, J.S. Liu, Bi_2WO_6 micro/nanostructures: synthesis, modifications and visible-light-driven photocatalytic applications, Appl. Catal. B: Environ. 106 (2011) 1–13.
[9] T. Saison, N. Chemin, C. Chaneac, O. Durupthy, V. Ruaux, L. Mariey, F. Mauge, P. Beaunier, J.P. Jolivet, Bi_2O_3, $BiVO_4$, and Bi_2WO_6: impact of surface properties on photocatalytic activity under visible light, J. Phys. Chem. C 115 (2011) 5657–5666.
[10] J.Q. Yu, Y. Zhang, A. Kudo, Synthesis and photocatalytic performances of $BiVO_4$ by ammonia co-precipitation process, J. Solid State Chem. 182 (2009) 223–228.
[11] W. Liu, M.S. Ji, S.F. Chen, Preparation, characterization and activity evaluation of $Ag_2Mo_4O_{13}$ photocatalyst, J. Hazard. Mater. 186 (2011) 2001–2008.
[12] K. Maeda, K. Teramura, D.L. Lu, T. Takata, N. Saito, Y. Inoue, K. Domen, Photocatalyst releasing hydrogen from water, Nature 440 (2006) 295.
[13] Z.G. Yi, J.H. Ye, N. Kikugawa, T. Kako, S. Ouyang, H.S. Williams, H. Yang, J.Y. Cao, W.J. Luo, Z.S. Li, Y. Liu, R.L. Withers, An orthophosphate semiconductor with photooxidation properties under visible-light irradiation, Nat. Mater. 9 (2010) 559–564.
[14] C.W. Xu, Y.Y. Liu, B.B. Huang, H. Li, X.Y. Qin, X.Y. Zhang, Y. Dai, Preparation, characterization, and photocatalytic properties of silver carbonate, Appl. Surf. Sci. 257 (2011) 8732–8736.
[15] X.G. Ma, B. Lu, D. Li, R. Shi, C.S. Pan, Y.F Zhu, Origin of photocatalytic activation of silver orthophosphate from first-principles, J. Phys. Chem. C 115 (2011) 4680–4687.
[16] C.T. Dinh, T.D. Nguyen, F. Kleitz, T.O. Do, Large-scale synthesis of uniform silver orthophosphate colloidal nanocrystals exhibiting high visible light photocatalytic activity, Chem. Commun. 47 (2011) 7797–7799.
[17] Y.P. Bi, S.X. Ouyang, N. Umezawa, J.Y. Cao, J.H. Ye, Facet effect of single-crystalline Ag_3PO_4 sub-microcrystals on photocatalytic properties, J. Am. Chem. Soc. 133 (2011) 6490–6492.
[18] Y.P. Bi, S.X. Ouyang, J.Y. Cao, J.H. Ye, Facile synthesis of rhombic dodecahedral AgX/Ag_3PO_4 (X = Cl, Br, I) heterocrystals with enhanced photocatalytic properties and stabilities, Phys. Chem. Chem. Phys. 13 (2011) 10071–10075.

[19] P. Wang, B.B. Huang, X.Y. Qin, X.Y. Zhang, Y. Dai, J.Y. Wei, M.H. Whangbo, Ag@AgCl: a highly efficient and stable photocatalyst active under visible light, Angew. Chem. Int. Ed. 47 (2008) 7931–7933.
[20] H. Xu, H.M. Li, J.X. Xia, S. Yin, Z.J. Luo, L. Liu, L. Xu, One-pot synthesis of visible-light-driven plasmonic photocatalyst Ag/AgCl in ionic liquid, ACS Appl. Mater. Interfaces 3 (2011) 22–29.
[21] C.H. An, S. Peng, Y.G. Sun, Facile synthesis of sunlight-driven AgCl:Ag plasmonic nanophotocatalyst, Adv. Mater. 22 (2010) 2570–2574.
[22] L. Han, P. Wang, C.Z. Zhu, Y.M. Zhai, S.J. Dong, Facile solvothermal synthesis of cube-like Ag@AgCl: a highly efficient visible light photocatalyst, Nanoscale 3 (2011) 2931–2935.
[23] L. Kuai, B.Y. Geng, X.T. Chen, Y.Y. Zhao, Y.C. Luo, Facil subsequently light-induced route to highly efficient and stable sunlight-driven Ag-AgBr plasmonic photocatalyst, Langmuir 26 (2010) 18723–18727.
[24] P. Wang, B.B. Huang, X.Y. Zhang, X.Y. Qin, H. Jin, Y. Dai, Z.Y. Wang, J.Y. Wei, J. Zhan, S.Y. Wang, J.P. Wang, M.H. Wangbo, Highly efficient visible-light plasmonic photocatalyst Ag@AgBr, Chem. Eur. J. 15 (2009) 1821–1824.
[25] X.H. Huang, I.H. El-Sayed, W. Qian, M.A. El-Sayed, Cancer cell imaging and photothermal therapy in the near-infrared region by using gold nanorods, J. Am. Chem. Soc. 128 (2006) 2115–2120.
[26] C. Langhammer, Z. Yuan, I. Zoric, B. Kasemo, Plasmonic properties of supported Pt and Pd nanostructures, Nano Lett. 6 (2006) 833–838.
[27] K. Awazu, M. Fujimaki, C. Rockstuhl, J. Tominaga, H. Murakami, Y. Ohki, N. Yoshida, T. Watanabe, A plasmonic photocatalyst consisting of silver nanoparticles embedded in titanium dioxide, J. Am. Chem. Soc. 130 (2008) 1676–1680.
[28] X. Chen, H.Y. Zhu, J.C. Zhao, Z.F. Zheng, X.P. Gao, Visible-light-driven oxidation of organic contaminants in air with gold nanoparticle catalysts on oxide supports, Angew. Chem. Int. Ed. 47 (2008) 5353–5356.
[29] J. Cao, B.D. Luo, H.L. Lin, S.F. Chen, Synthesis, characterization and photocatalytic activity of $AgBr/H_2WO_4$ composite photocatalyst, J. Mol. Catal. A: Chem. 344 (2011) 138–144.
[30] G.T. Li, K.H. Wong, X.W. Zhang, C. Hu, J.C. Yu, R.C.Y. Chan, P.K. Wong, Degradation of Acid Orange 7 using magnetic AgBr under visible light: the roles of oxidizing species, Chemosphere 76 (2009) 1185–1191.
[31] N. Zhang, S.Q. Liu, X.Z. Fu, Y.J. Xu, Synthesis of M@TiO_2 (M = Au, Pd, Pt) core-shell nanocomposites with tunable photoreactivity, J. Phys. Chem. C 115 (2011) 9136–9145.
[32] Y.Y. Li, J.S. Wang, H.C. Yao, L.Y. Dang, Z.J. Li, Efficient decomposition of organic compounds and reaction mechanism with BiOI photocatalyst under visible light irradiation, J. Mol. Catal. A: Chem. 334 (2011) 116–122.
[33] K. Ishibashi, A. Fujishima, T. Watanabe, K. Hashimoto, Detection of active oxidative species TiO_2 photocatalysis using the fluorescence technique, Electrochem. Commun. 2 (2000) 207–210.
[34] Q. Xiao, Z.C. Si, J. Zhang, C. Xiao, X.K. Tan, Photoinduced hydroxyl radical and photocatalytic activity of samarium-doped TiO_2 nanocrystalline, J. Hazard. Mater. 150 (2008) 62–67.
[35] J. Cao, B.D. Luo, H.L. Lin, B.Y. Xu, S.F. Chen, Thermodecomposition synthesis of WO_3/H_2WO_4 heterostructures with enhanced visible light photocatalytic properties, Appl. Catal. B: Environ. 111–112 (2012) 288–296.
[36] H. Zhang, G. Wang, D. Chen, X.J. Lv, J.H. Li, Tuning photoelectrochemical performances of Ag-TiO_2 nanocomposites via reduction/oxidation of Ag, Chem. Mater. 20 (2008) 6543–6549.
[37] Y.P. Liu, L. Fang, H.D. Lu, L.J. Liu, H. Wang, C.Z. Hu, Highly efficient and stable Ag/Ag_3PO_4 plasmonic photocatalyst in visible light, Catal. Commun. 17 (2012) 200–204.
[38] S.X. Liu, Z.P. Qu, X.W. Han, C.L. Sun, X.H. Bao, Effect of silver deposition on photocatalytic activity of TiO_2, Chin. J. Catal. 25 (2004) 133–137.
[39] C. Tabor, R. Murali, M. Mahmoud, M.A. El-Sayed, On the use of plasmonic nanoparticle pairs as a plasmon ruler: the dependence of the near-field dipole plasmon coupling on nanoparticle size and shape, J. Phys. Chem. A 113 (2009) 1946–1953.
[40] M.A. Butler, Photoelectrolysis and physical properties of the semiconducting electrode WO_2, J. Appl. Phys. 48 (1977) 1914–1920.
[41] H. Wang, J. Gao, T.Q. Guo, R.M. Wang, L. Guo, Y. Liu, J.H. Li, Facile synthesis of AgBr nanoplates with exposed {1 1 1} facets and enhanced photocatalytic properties, Chem. Commun. 48 (2012) 275–277.
[42] X. Zhang, L.Z. Zhang, T.F. Xie, D.J. Wang, Low-temperature synthesis and high visible-light-induced photocatalytic activity of BiOI/TiO_2 heterostructures, J. Phys. Chem. C 113 (2009) 7371–7378.
[43] C.C. Chen, W.H. Ma, J.C. Zhao, Semiconductor-mediated photodegradation of pollutants under visible-light irradiation, Chem. Soc. Rev. 39 (2010) 4206–4219.
[44] C.S. Pan, Y.F. Zhu, New type of BiPO4 oxy-acid salt photocatalyst with high photocatalytic activity on degradation of dye, Environ. Sci. Technol. 44 (2010) 5570–5574.
[45] H.F. Cheng, B.B. Huang, Y. Dai, X.Y. Qin, X.Y. Zhang, One-step synthesis of the nanostructured AgI/BiOI composites with highly enhanced visible-light photocatalytic performance, Langmuir 26 (2010) 6618–6624.
[46] H. Tang, K. Prasad, R. Sanjines, P.E. Schmid, F. Levy, Electrical and optical properties of TiO_2 anatase thin films, J. Appl. Phys. 75 (1994) 2042–2047.
[47] X.F Zhou, C. Hu, X.X. Hu, T.W. Peng, J.H. Qu, Plasmon-assisted degradation of toxic pollutants with Ag-AgBr/Al_2O_3 under visible-light irradiation, J. Phys. Chem. C 114 (2010) 2746–2750.
[48] Y.Q. Yang, G.K. Zhang, S.J. Yu, X. Shen, Efficient removal of organic contaminants by a visible light driven photocatalyst $Sr_6Bi_2O_9$, Chem. Eng. J. 162 (2010) 171–177.
[49] J. Kim, C.W. Lee, W. Choi, Platinized WO_3 as an environmental photocatalyst that generates OH radicals under visible light, Environ. Sci. Technol. 44 (2010) 6849–6854.
[50] S. Meng, D.Z. Li, M. Sun, W.J. Li, J.X. Wang, J. Chen, X.Z. Fu, G.C. Xiao, Sonochemical synthesis, characterization and photocatalytic properties of a novel cube-shaped $CaSn(OH)_6$, Catal. Commun. 12 (2011) 972–975.
[51] W.M. Wu, S.J. Liang, Y. Chen, L.J. Shen, H.R. Zheng, L. Wu, High efficient photocatalytic reduction of 4-nitroaniline to p-phenylenediamine over microcrystalline $SrBi_2Nb_2O_9$, Catal. Commun. 17 (2012) 39–42.
[52] J. Bandara, J. Kiwi, Fast kinetic spectroscopy, decoloration and production of H_2O_2 induced by visible light in oxygenated solutions of the azo dye Orange II, New J. Chem. 23 (1999) 717–724.
[53] M.C. Yin, Z.S. Li, J.H. Kou, Z.G. Zou, Mechanism investigation of visible light-induced degradation in a heterogeneous TiO_2/Eosin Y/Rhodamine B system, Environ. Sci. Technol. 43 (2009) 8361–8366.
[54] D.T. Sawyer, J.S. Valentine, How super is superoxide? Acc. Chem. Res. 14 (1981) 393–400.
[55] T. Tatsuma, K. Takada, T. Miyazaki, UV-light-induced swelling and visible-light-induced shrinking of a TiO_2-containing redox gel, Adv. Mater. 19 (2007) 1249–1251.
[56] M. Antoniadou, P. Lianos, Production of electricity by photoelectrochemical oxidation of ethanol in a PhotoFuelCell, Appl. Catal. B: Environ. 99 (2010) 307–313.
[57] H. Ueno, J. Nemoto, K. Ohnuki, M. Horikawa, M. Hoshino, M. Kaneko, Photoelectrochemical reaction of biomass-related compounds in a biophotochemical cell comprising a nanoporous TiO_2 film photoanode and an O_2-reducing cathode, J. Appl. Electrochem. 39 (2009) 1897–1905.
[58] H. Liu, W.R. Cao, Y. Su, Y. Wang, X.H. Wang, Synthesis, characterization and photocatalytic performance of novel visible-light-induced Ag/BiOI, Appl. Catal. B: Environ. 111–112 (2012) 271–279.
[59] P. Wang, B.B. Huang, X.Y. Qin, X.Y. Zhang, Y. Dai, M.H. Whangbo, $Ag/AgBr/WO_3 \cdot H_2O$: visible-light photocatalyst for bacteria destruction, Inorg. Chem. 48 (2009) 10697–10702.
[60] W.W. Lu, S.Y. Gao, J.J. Wang, One-pot synthesis of Ag/ZnO self-assembled 3D hollow microspheres with enhanced photocatalytic performance, J. Phys. Chem. C 112 (2008) 16792–16800.
[61] M. Sadeghi, W. Liu, T.G. Zhang, P. Stavropoulos, B. Levy, Role of photoinduced charge carrier separation distance in heterogeneous photocatalysis: oxidative degradation of CH_3OH vapor in contact with Pt/TiO_2 and cofumed TiO_2-Fe_2O_3, J. Phys. Chem. 100 (1996) 19466–19474.